Selection rules and dispersion of GaAs/AlAs multiple-quantum-well optical phonons studied by Raman scattering in right-angle, forward, and backscattering in-plane geometries

A. Fainstein, P. Etchegoin,* M. P. Chamberlain, M. Cardona, K. Tötemeyer, and K. Eberl
Max-Planck-Institut für Festkörperforschung, Heisenbergstrasse 1, 70569 Stuttgart, Germany
(Received 1 December 1994)

We present a detailed experimental study of optical phonon Raman scattering in GaAs/AlAs multiple quantum wells for several in-plane geometries. By exploiting a waveguided structure, we performed 90°, forward, and backscattering experiments with dispersed light propagating *along* the layers. Using these geometries, phonons with various propagation directions and polarized both parallel and perpendicular to the growth axis can be probed. The 90° data complete and correct earlier results obtained for the same geometry by Zucker *et al.*, bringing them into accord with later experimental and theoretical work. Moreover, in-plane forward scattering data are reported as a complementary check to these experiments. We discuss selection rules and scattering mechanisms, and compare the results with phonon energies calculated within a continuum model based on linear combinations of LO, TO, and interface modes. We find a very good agreement between the experiment and the predictions of the established theory of phonon modes and Raman scattering in semiconductor heterostructures.

I. INTRODUCTION

Optical phonons in semiconductor multiple quantum wells (MQW's) and the light scattering from them has been intensively studied in the last ten years, and already many review articles summarizing both experimental and theoretical results can be found in the literature.[1–4] However, Raman experiments that directly probe in-plane dispersion are rare.[5–8] By exploiting a waveguided structure we have investigated Raman scattering geometries where one or both of the incident and scattered photons propagate parallel to the MQW layers. Up until now, and to the best of our knowledge, only one such experiment in a 90° geometry has been reported[9] and none for in-plane forward scattering.

The optical vibrations of semiconductor MQW's resemble in many aspects those of a stacking of thin ionic slabs.[10–12] This is especially true when the optical phonon branches of the consecutive layers do not overlap, as happens for GaAs/AlAs MQW's. In this case, similar to that for electrons, the vibrational modes remain confined in either slab. This confinement is the counterpart of the "folding" of acoustic vibrations[13] and leads to a series of phonons labeled by an integer m, which are called *confined optical modes.*[14,15] The effect of the MQW periodicity on the GaAs confined optical modes may be viewed as equivalent to considering bulk phonons but with a wave-vector component in the z direction (along the growth axis) given by $q_z + m\pi/d_1$, where d_1 is the GaAs well thickness and $m = 1, 2, 3...$.[12,15] Thus, for $q_z \ll q_\perp \ll m\pi/d_1$, where $q_\perp$ is the component of the phonon crystal momentum perpendicular to z, these vibrations have, generally speaking, the remarkable property that z-polarized modes have LO-like frequency, while in-plane polarized modes have TO-like frequency, independent of their propagation direction.

This latter feature of the MQW confined optical phonon modes was first demonstrated by Zucker *et al.* in 1984 (Ref. 9) in an experiment revealing the excitation of phonons with LO frequencies but with Raman selection rules characteristic of TO modes. This experiment was performed in a 90° geometry on a $GaAs/Al_{0.28}Ga_{0.72}As$ MQW enclosed by cladding layers which form a waveguide for the scattered light. The right-angle geometry enabled the observation of light scattered by phonons with a finite $q_\perp$, both with polarization *along* and perpendicular to z. Note that, due to the extremely small thickness of the artificially grown MQW's (≈ 1 μm), experiments in which either the incident or the scattered light come to, or from, the side, are rare, and Raman scattering experiments are usually performed in backscattering geometry along z. This geometry only allows, for first-order processes, the excitation of phonons with zero in-plane momentum. Only the development of micro-Raman techniques has made possible the investigation of backscattering geometries where the momentum transfer can be in any direction between the growth and in-plane directions.[5–8]

These micro-Raman experiments[5–8] together with previous experimental[16] and theoretical work[17–21] (for a complete list see Refs. 8 and 20) showed that the nature of the phonon modes in polar semiconductor MQW's is much more complicated than a simple folding of the bulk dispersions. In fact, besides the above modification of the bulk optical phonons due to the new periodicity along z, the stacking of layers in a MQW produces other changes in the long-range part of the Coulomb forces as compared to the bulk. The complex characteristics of the resulting phonon modes can be visualized by analyzing their angular dispersion with respect to the angle Θ between z and the phonon wave vector $\vec{q}$, for a fixed

magnitude q (normally taken to be of the order of the "transfer q" in a Raman experiment). Confined modes of *even* index m do *not* show angular dispersion respect to Θ. On the contrary, *odd* order modes show a more complicated behavior: the $m = 1$ LO (or TO) -like mode develops a downward (upward) angular dispersion and anticrosses with the other confined modes of equal symmetry (odd m).[19,20] The $m = 1$ strongly dispersive modes correspond to those termed *interface modes* in early dielectric continuum models.[4,13,16] The name is related to the fact that, in those models and for finite $q_\perp$ their amplitude decays exponentially away from the interfaces.[4] Notice that their identification as "interface modes" may be misleading since it seems to imply the existence of modes other than the confined ones. Nevertheless, and for historical reasons and the sake of shortness, we stick to the widely used assignment of the $m = 1$ LO (TO) modes as upper (lower) interface modes (IF). In Ref. 8 the complete angular dispersion of the phonon modes of GaAs/AlAs (7/7) and (12/12) MQW's was determined using the micro-Raman technique and compared to the continuum theory of Ref. 20.

The main result of the Raman scattering experiment reported earlier by Zucker *et al.*,[9] i.e., the fact that in general z polarized modes vibrate at LO-like frequencies regardless of their propagation direction (with the exception of the $m = 1$/interface modes), was confirmed by later micro-Raman experiments.[5–8] However, many other important features of the data of Ref. 9, particularly selection rules, phonon energies, and scattering mechanisms, have been shown to be inconsistent with theoretical findings[17–21] and other experiments.[5–8,16] Let us illustrate these points: (i) according to Raman scattering selection rules,[22] the TO-like peaks observed in $z(y',z)y'$ and $z(x',z)y'$ configurations (as usual, the incident and scattered polarizations are indicated inside the brackets and $[1\bar{1}0]$ is defined as the in-plane direction of the scattered light y') should represent two different types of TO modes, one which shows angular dispersion and the other which does not.[21] This difference was *not* resolved in Ref. 9. (ii) A strong peak at the bulk LO frequency was observed for $z(x',x')y'$ configuration while the LO_1 mode is expected to reduce its frequency in 90° scattering due to the angular dispersion of interface modes. (iii) Strong scattering was reported for $z(y',x')y'$ configuration which is forbidden by symmetry. (iv) It was concluded that the Raman tensor is invariant under rotations about the superlattice axis, something that contradicts the symmetry-derived selection rules for the D_{2d} group of GaAs/AlAs MQW's.

However, the experiments of Ref. 9, performed ten years ago, have so far remained unchallenged. Because of the disagreement already outlined we have carried out a detailed experimental study of the Raman scattering spectra of GaAs/AlAs MQW's in a series of in-plane scattering configurations involving 90°, forward and backscattering. Similar to the sample used in Ref. 9, we used a waveguided MQW to efficiently collect light scattered in the in-plane direction. However, we studied thinner quantum wells to make the confinement effects more clear (51.5 Å in our case against, 96 Å in Ref. 9). Also, because the effect of two-mode behavior of the alloys on the MQW phonons is not well understood,[23] we worked with AlAs instead of $Al_{0.28}Ga_{0.72}As$ barriers.

We performed 90° Raman scattering experiments with excitation along z and light collected along both [110] and [100]. Contrary to Ref. 9, we find the two series of spectra to be different and, in fact, to be consistent with the expected selection rules. We find good agreement of the observed spectra with the optical phonon energies derived from a continuum model calculation which takes into account the mixing of LO, TO, and interface modes.[20] The intensity of the observed peaks is also in accord with the scattering mechanism (Fröhlich or deformation potential) involved for each configuration.[15]

To check these findings for other in-plane geometries, we performed forward scattering experiments with the incident and scattered light propagating *along* the plane of the quantum wells. Up until now only forward scattering along the growth direction, for which the substrate has to be removed to avoid absorption, had been reported for semiconductor MQW's.[24] In addition to the waveguide design of our sample making the collection of light rather efficient, the large scattering volume achieved when measuring below the absorption edge of the sample helps to make in-plane forward scattering experiments possible. We studied scattering with light incident along both [110] and [100] directions. As for the right-angle spectra, we find selection rules, phonon energies, and peak amplitudes in accordance with the established theory.

For the sake of completeness, we also performed backscattering experiments with light incident along the plane of the layers, similar to those reported in Refs. 5–8. The results agree well with those obtained for the other geometries. Only some minor departures from the expected selection rules, also reported in Ref. 6, are observed for the data obtained in the green spectral region, probably due to resonance effects.

The paper is organized as follows. In Sec. II we present an overview of the theory required to analyze the data, namely phonon dispersions, selection rules, and scattering mechanisms. In Sec. III we describe the samples and experimental setup. Section IV presents our experimental results for the three studied geometries: 90°, forward, and backscattering, together with a discussion of the data in terms of the expected selection rules and phonon energies derived from a continuum model calculation. The conclusions are given in Sec. V.

II. THEORETICAL OVERVIEW

A. Angular dispersion of optical phonons

Although an accurate description of the angular dispersion of optical modes first became possible within the framework of microscopic phonon models,[17–19] it was shown recently that results with similar accuracy can also be obtained with a modified continuum model.[20] In this model, the dependence of the phonon energy on the wave vector is modeled by assuming isotropic and

parabolic bands, and the optical phonons are described as linear combinations of LO, TO, and interface modes which satisfy both mechanical and electrostatic boundary conditions at the interfaces. We use this modified continuum model which, compared to microscopic models, needs only a small computational effort since analytical solutions are obtained.

In Fig. 1 we show the angular dispersion of the GaAs-like optical phonon modes of a GaAs/AlAs (51.5/48 Å) MQW, calculated for a phonon wave vector 9.56×10^4 cm^{-1} which corresponds approximately to the wave vector transferred in our right-angle experiments. The angle Θ is defined between z and the phonon wave vector which, for $\Theta = 90°$, is aligned parallel to y . Since in the model rigid barriers are assumed at the interfaces, the GaAs-like modes of the GaAs/AlAs (18/16 monolayers) MQW are actually modeled with a (19/15 monolayers) MQW in order to account for the displacement of the As atoms at the interfaces.[8,20]

From Fig. 1 it can be seen that as the direction of $\vec{q}$ rotates away from z strongly angular dispersing modes evolve out of the $m = 1$ LO and TO modes (the so-called "interface modes"). The LO_1 frequency decreases while the TO_1 splits into two branches, one dispersionless (polarized along x) and the other with an upward dispersion (polarized along y). Whenever the dispersive modes' frequencies approach that of a mode with the same symmetry (i.e., an odd numbered mode), the two modes mix, i.e., anticross.[8,19,20] For $\Theta \neq 0$ this mixing results in modes which are linear combinations of modes polarized both along z and y, thus prohibiting a meaningful classification in terms of polarization and mode number. Nevertheless, and for identification purposes, we will label them by their classification at $\Theta = 0$. The $m = 1$ modes show the largest angular dispersion because their amplitude is nodeless within the GaAs region and consequently they carry the largest dipole moment. On the other hand, the positive and negative lobes in the diplacement pattern of *even* order modes cancel exactly and therefore they do not generate a macroscopic electric field. Consequently, even numbered modes remain dispersionless. Strictly speaking this picture only holds for $q \to 0$: for $q \neq 0$ the classification in terms of odd and even modes is not possible, leading to small mixing and hence weak anticrossings also with the even order modes.[20]

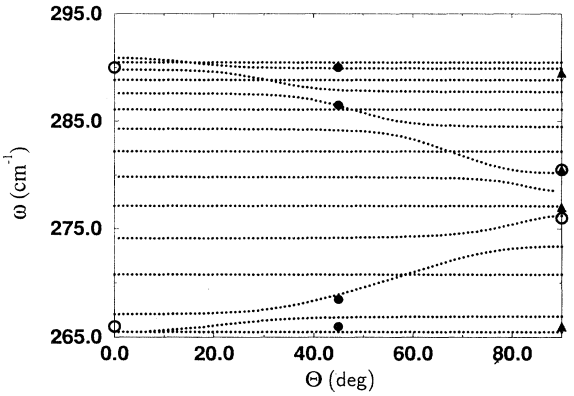

FIG. 1. Angular dispersion of the GaAs-like optical phonon modes of a GaAs/AlAs (18/16) MQW calculated with the extended continuum model of Ref. 17. The dispersion relations were actually modeled with a (19/15) MQW in order to account for the displacements of the As atoms at the interfaces. The TO and LO bulklike frequencies were taken as 265.5 cm^{-1} and 291 cm^{-1}, respectively. The calculation is for $q = 9.56 \times 10^4$ cm^{-1} which corresponds approximately to right-angle scattering. Θ is defined between z and the phonon wave vector $\vec{q}$, which for $\Theta = 90°$ is aligned with y. Experimental points, discussed in Sec. IV, are indicated in the figure by full circles (for right-angle scattering), empty circles (for forward scattering) and full triangles (for backscattering). In the figures to come (Figs. 3, 4, 5, and 8), we use the same symbols to label the peaks displayed here as experimental points to facilitate the identification. Each different phonon, when observed in more than one configuration, appears at the same frequency within the experimental resolution.

B. Raman tensors and selection rules

For $q = 0$ the phonon modes can be analyzed in terms of the irreducible representations of the crystal point group. In the D_{2d} point group of the GaAs/AlAs MQW's, the z vibrations belong either to the B_2 (m odd) or the A_1 (m even) representations. The in-plane polarized modes are described by the E representations.[25]

The corresponding allowed Raman tensors, in the basis $[100] = \hat{x}$, $[010] = \hat{y}$, and $[001] = \hat{z}$, read[22,25]

$$\mathbf{R}_{B_2(z)} = \begin{pmatrix} 0 & d & 0 \\ d & 0 & 0 \\ 0 & 0 & 0 \end{pmatrix}, \quad \mathbf{R}_{A_1} = \begin{pmatrix} a & 0 & 0 \\ 0 & a & 0 \\ 0 & 0 & b \end{pmatrix} \tag{1}$$

for the z polarized modes and

$$\mathbf{R}_{E(x)} = \begin{pmatrix} 0 & 0 & 0 \\ 0 & 0 & e \\ 0 & e & 0 \end{pmatrix}, \quad \mathbf{R}_{E(y)} = \begin{pmatrix} 0 & 0 & e \\ 0 & 0 & 0 \\ e & 0 & 0 \end{pmatrix} \tag{2}$$

for the in-plane vibrations.

The scattering efficiency is given by[22,25]

$$\frac{dS}{d\Omega} \propto |\hat{e}_L \cdot \mathbf{R} \cdot \hat{e}_S|^2 , \tag{3}$$

where $\hat{e}_L$ and $\hat{e}_S$ are the polarization directions of incident and scattered fields.

We should point out that the discussion above is based on the assumption that q is *exactly* zero. This approximation must be analyzed with some care in cases where a finite non-negligible $\vec{q}$ actually means a serious reduction of the overall symmetry of the case $q = 0$. The fact that $\vec{q}$ cannot always be set to zero is perhaps most obvious for Brillouin scattering, for which $q = 0$ implies a rigid translation of the system and hence no modulation of the dielectric function. Also, *straightforward* application of this approximation for interpreting spectra of

optical phonons in polar MQW's is by no means justified since, although no large spatial dispersion effects are expected in this case, a finite q sets up macroscopic electric fields which lower the symmetry. Consequently, the modes may no longer belong to a D_{2d} representation and thus Eqs. (1) and (2) may not hold. For backscattering along z the symmetry is still D_{2d} and hence use of the $q = 0$ approximation is correct. For in-plane backscattering along [100] or [110] the symmetry is reduced to the orthorhombic D_2 or C_{2v} point groups, respectively. The normal modes of vibration are still x, y, or z polarized (or along primed axes in case of propagation along [110]). The Raman tensors look much the same as for D_{2d} symmetry,[22] except for the fact that the coefficients in the $E(x)$-like and $E(y)$-like tensors are *not* equal. This change reflects the lifting of degeneracy between x- and y-polarized vibrations, evident in the angular dispersion shown in Fig. 1. Also evident in Fig. 1 is the fact that for intermediate values of Θ the eigenmodes are *not* pure y or z polarized implying a further reduction of symmetry. Moreover, they are *not* of pure LO or TO character: electrostatic boundary conditions at the GaAs/AlAs interfaces add to the macroscopic electric field generated along $\vec{q}$ resulting in a mixture of both components. For propagation along the $z-y$ or $z-y'$ planes (with $\Theta \neq 0°, 90°$) the q-vector point groups are the monoclinic C_2 or C_s, respectively. The reduction of symmetry for these crystal groups results in the fact that the Raman tensors for y- and z-polarized modes (with different nonvanishing components) do not exist any more and are replaced by a tensor belonging to the so-called B representation. Therefore, the phonon modes and selection rules should be analyzed for each scattering geometry according to the respective group of the q vector. However, the symmetry of the modes and selection rules for $q = 0$ give physical insight into which modes should mix, or are expected to scatter, for each configuration. We will, therefore, give the selection rule at $q = 0$ [given by Eqs. (1) and (2)] when presenting the data, together with the expected character of the mode taking into account the reduced symmetry due to the effect of the macroscopic electric field.

As an example, consider the right-angle geometry configurations $z(y,z)y$ and $z(x,z)y$. Equations (1)–(3) imply that each configuration will only couple to $E(x)$ or $E(y)$ modes, i.e., vibrations polarized along x and y, respectively. Considering that the $\vec{q}$ transfer will be directed at 45° with respect to z, and resorting to Fig. 1, we see that pure x-polarized modes exist at the bulklike TO frequency, while both "interface modes" are partially y polarized. Consequently, for the first configuration [$E(x)$ allowed modes for $q = 0$] the spectrum should consist of a pure TO peak, fixed at the energy of the bulklike TO phonon. On the other hand, for the second configuration [$E(y)$ allowed modes for $q = 0$], the main peak should correspond to a TO-like phonon displaced by about 3.3 cm^{-1} to higher energies with respect to the bulklike frequency, plus scattering at the energy of the upper "interface mode" (LO-like).

Note also that even in the $q = 0$ approximation the Raman tensors are strongly anisotropic for rotations about

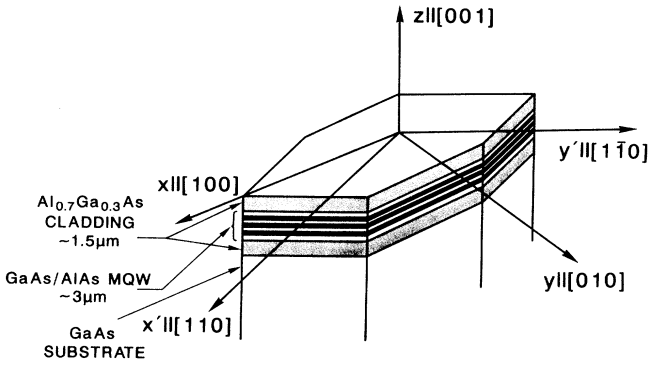

FIG. 2. Schematic of the sample and the coordinate systems used. The sample consists of a thick ($\approx$ 2.8 μm) GaAs/AlAs MQW (300 times 51.5 Å/46 Å) enclosed by $\approx$ 1.5 μm $Al_{0.7}Ga_{0.3}As$ layers. The refractive index of the cladding is smaller than that of the MQW so that light guiding occurs. The axes [110] (x') and [1$\bar{1}$0] (y') are perpendicular to cleavage planes. Some samples were polished perpendicular to the crystalline axes [100] (x) or [010] (y).

z. In fact, if we define the primed coordinate system $(x'y'z)$ as in Fig. 2, with x' along [110], it is easy to see that a $z(y,x)y$ configuration couples to B_2-like modes while the $z(y',x')y'$ should couple to none.

C. Scattering mechanisms

In bulk polar semiconductors the electron-phonon interaction can be separated into a long- and a short-range part:[26]

$$H_{e\text{-ph}} = H_F + H_{\mathrm{DP}}. \tag{4}$$

The long-range part is the Fröhlich interaction, which is induced by the macroscopic electric fields created by longitudinal phonons ($H_F \propto 1/q$). On the other hand, the short-range part corresponds to the deformation-potential interaction, also found in nonpolar materials such as Si and Ge.

The bulklike deformation-potential operator H_{DP} produces the Raman tensors $R_{E(x)}$, $R_{E(y)}$, and $R_{B_2(z)}$ of Eqs. (1) and (2). On the other hand, a diagonal tensor like the one corresponding to A_1 phonons can be derived for bulk polar semiconductors from Fröhlich-interaction-induced scattering.[25,27] The efficiency for this latter scattering is proportional to the square of q, thus being "dipole-forbidden" (quadrupole allowed). Although the wave vector q is actually very small in a first-order light scattering process, Fröhlich intraband processes can give strong resonant contributions to the Raman efficiency.[28] Moreover, by allowing large q's, impurity-scattering processes may enhance the scattering cross section despite being a second-order mechanism.[27]

These mechanisms existing in bulk materials may be carried over to MQW's. Note, however, that the q-

dependent Fröhlich mechanism only applies to *odd* numbered confined modes because the *even* ones do not carry a macroscopic electric field. On the other hand, besides these two mechanisms existing in bulk materials, scattering in MQW's may also occur mediated by the large electrostatic potential accompanying the confined optical modes and due to the charge induced at the GaAs/AlAs interfaces. Depending on the well width, the length scale of this potential resembles more that of a Fröhlich-type or of a deformation-potential-type mechanism. This mechanism has been considered for intraband processes in Ref. 15 in a similar way to which "q-Fröhlich" scattering is evaluated in the bulk. It was shown there that it becomes dipole allowed in MQW's because q in the electrostatic potential is replaced by the much larger "confinement" wave vector $m\pi/d$. By being intraband, this "π/d-Fröhlich" mechanism also leads to a diagonal tensor like that for A_1 phonons. Moreover, only A_1 symmetry phonons (*even* number) can be scattered by this mechanism due to their even electrostatic potential.[15]

Both B_2 (m odd) and A_1 (m even) z vibrations have been identified in Raman scattering experiments (see, for example, Refs. 14 and 15). It was shown that away from resonance the deformation-potential terms dominate (m odd),[14] but in resonance the π/d-Fröhlich contribution is stronger (m even).[15]

III. SAMPLES AND EXPERIMENTAL SETUP

In order to transmit and collect light along the MQW layers, a sample having a symmetric waveguide structure was grown by molecular-beam epitaxy (MBE) on an undoped [001]-oriented GaAs substrate. The waveguide core was composed of a MQW consisting of 300 periods of GaAs/AlAs (18/16 monolayers), amounting to a total width of about 2.8 μm, sandwiched between two 1.5 μm $Al_{0.7}Ga_{0.3}As$ cladding layers (see Fig. 2). Since the refractive index is larger in the MQW than in the cladding, light rays propagating at grazing incidence in the MQW undergo total internal reflection and thus light guiding is acomplished.[29,30] Previously, Raman scattering,[9] absorption,[31] polariton time of flight,[32] and birefringence[33] experiments have exploited similar waveguide structures to probe in-plane properties of semiconductor MQW's. The period of our MQW (97.5 Å) was determined by x-ray diffraction and also from the Raman backscattering by acoustic folded phonons. The room-temperature gap (heavy hole to conduction band) of this sample was found from luminescence measurements to be 1.567 eV. Figure 2 shows a diagram of the sample together with the coordinate systems used. Geometries with light propagating along both [110] or [100] directions were studied with cleaved or polished sample surfaces, respectively.

For the backscattering experiments, and due to our observation of small Raman signals originating in the $Al_{0.7}Ga_{0.3}As$ alloy cladding, we relied on a similar but unclad sample. This second sample consisted of 300 periods of GaAs/AlAs (15/15 monolayers), amounting to a total width of about 2.3 μm, directly grown on a [001]-oriented GaAs substrate. Measurements were performed on a (110) cleaved face. The room-temperature luminescence gap of this sample was 1.633 eV, somewhat larger than that of the clad sample due to the smaller well width.

A pumped Ti-sapphire laser was used to excite the spectra for the 90° and forward scattering experiments in the frequency range 1.5–1.54 eV, *below* the MQW gap. The beam was focused with a lens ($f \approx 10$ cm) on the (001) face (for the 90° experiments) or on the side face of the sample where the waveguide was located (for the forward scattering geometry). The size of the laser spot is not a strong experimental requirement in either the 90° or the forward scattering geometry since, for frequencies above the energy gap of the GaAs substrate (1.37 eV) and below that of the MQW (1.567 eV), light propagates only through the MQW and hence no microfocusing is required. Only careful masking is needed in both cases to limit stray light which would affect the collection of inelastically scattered light. For both geometries the outgoing light was collected with a 5 cm focal length lens, limiting the angles of the scattered light inside the sample to about 7° around the lens axis. The collected light was later passed through a second polarizer, analyzed with a Jarrell-Ash model No. 25–100 double monochromator provided with 590 lines/mm gratings blazed at 10 000 cm^{-1}, and finally detected with a GaAs photomultiplier by conventional photon counting. Due to the polarization dependence of the monochromator throughput (about 8:1 in the studied energy range) a polarization rotator was added before the slits of the monochromator in some experiments in order to measure both horizontal and vertical polarizations with the same dynamic range and signal-to-noise ratio.

The Raman spectra in backscattering configuration with $\vec{k}_i \parallel \vec{k}_s \parallel [1\bar{1}0]$ were collected using a Dilor triple spectrometer with a charge coupled device (CCD) multichannel detector. In order to avoid scattered light coming from the substrate, microfocusing must be used for this geometry. A built-in microscope with a $\times 100$ objective focuses and collects the light with spot sizes of about 1 μm. The excitation, above the gap of the MQW, was performed in this case using the discrete lines of an Ar^+-ion laser. All experiments were carried out at room temperature, with a resolution of about 1–2 cm^{-1}.

IV. EXPERIMENTAL RESULTS AND DISCUSSION

A. 90° scattering geometry

Figure 3 shows GaAs-like optical phonon Raman spectra for light incident along z and collected along y' ($[1\bar{1}0]$). Spectra for the four possible polarization configurations are shown and, for comparison, the position of the LO_1 phonon measured in usual backscattering geometry along the growth axis $[z(x',x')\bar{z}]$. Also, we present for the LO region of the two lower configurations similar right-angle Raman spectra collected along the perpendicular x' direction (dashed lines). For this case, the

lower curve corresponds to $z(y',z)x'$ configuration [$E(y')$ allowed scattering] and the upper to $z(x',z)x'$ [$E(x')$ allowed]. This figure should be compared with Fig. 1 of Ref. 9. The symmetry of the allowed modes for $q = 0$ is also given, together with the expected character of the vibrations as discussed in Sec. II B. Peak positions from spectra in Fig. 3 are indicated in Fig. 1 by full circles.

A first glance at the spectra shows that the main peak corresponding to the z-polarized allowed scattering is located in the LO region of the spectra while those of in-plane vibrations have frequencies in the TO range, in spite of the fact that the phonon $\vec{q}$ points at 45° with respect to z. This behavior, which resembles the vibrational properties of a thin ionic slab,[10] was first pointed out by Zucker *et al.*[9] A more careful second look at the data shows some other important details: (i) no scattering is observed for $z(y',x')y'$, contrary to Ref. 9, where the spectrum for this configuration was almost equal to that observed for $z(x',x')y'$; (ii) the Raman shift of the LO-like peak in the $z(x',x')y'$ configuration ($\approx$ 286.5 cm^{-1}) is smaller than that of the LO_1 mode obtained in a backscattering experiment along z ($\approx$ 290.7 cm^{-1}); (iii) the two lower spectra do not give the same result but, instead, the TO-like feature for $z(y',z)y'$ ($\approx$ 268.5 cm^{-1})

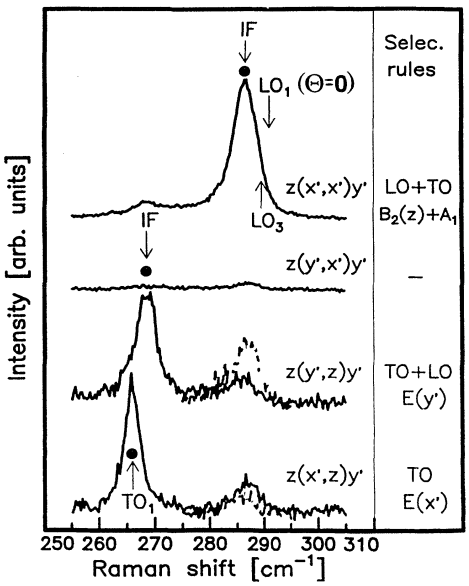

FIG. 3. Raman spectra in the right-angle geometry excited at a laser energy of 1.52 eV with a Ti-sapphire laser. Light is incident along z and collected from a (110) cleaved face (y'). The four possible configurations are shown, together with the predicted selection rules for $q = 0$ and the expected character of the modes, as discussed in Sec. II B. For comparison the LO_1 frequency (obtained in a backscattering experiment along z) is indicated. The dashed curves were obtained by similar right-angle Raman experiments but with light collected along the perpendicular x' direction (dashed lines). The lower dashed curve corresponds to $z(y',z)x'$ configuration [$E(y')$ allowed scattering, pure TO character] and the upper to $z(x',z)x'$ [$E(x')$ allowed, mixed LO+TO character].

shifts to a higher frequency with respect to that seen for $z(x',z)y'$ ($\approx$ 266 cm^{-1}); (iv) the TO-like peak observed in $E(y')$ allowed scattering is broader than that corresponding to the x'-polarized vibration [$E(x')$ allowed mode]; (v) smaller structures are also observed in the LO frequency range for the E symmetry allowed configurations and in the TO range for the $B_2(z) + A_1$ allowed one.

Point (i) above is expected simply from the selection rules derived from very general symmetry considerations. On the other hand, both selection rules and optical phonon angular dispersions (Fig. 1) must be considered to explain the other highlighted features. Let us discuss each of them separately.

(1) The $\vec{q}$ phonon wave vector transferred in right-angle scattering corresponds to $\Theta = 45°$ in Fig. 1. No signal at the LO_1 frequency (corresponding to $\Theta = 0°$, i.e., backscattering along z) is thus expected but, instead, the LO-like peak should shift to lower energies. In fact, comparing the experimental Raman shift with the calculated dispersion we find that it is close to the upper "interface mode." In principle, both Fröhlich and deformation-potential mediated scattering is allowed for the $z(x',x')y'$ configuration (i.e., odd *and* even modes may be excited). Nevertheless, is has been shown[14,15] (and will be confirmed below) that the deformation potential dominates except very close to resonance. Thus, it is understandable that LO_2 (and other even modes) does not contribute significantly to the scattering efficiency. The "interface" mode which derives from LO_1 has a nodeless displacement pattern within the GaAs region and thus provides the largest scattering intensity. The number of nodes in the displacement of confined modes increases with m. Consequently, their scattering efficiency decays as $1/m^2$ thus preventing the observation of high-order modes.[34,35] The high-energy shoulder of the LO-like peak in Fig. 3 may arise from scattering by LO_3 (as labeled).

(2) Configurations $z(x',z)y'$ and $z(y',z)y'$, corresponding to the two lower spectra in Fig. 3, couple to different TO-like modes polarized perpendicular and parallel to the $\vec{q} - z$ plane, respectively. According to Fig. 1 and the discussion in Sec. II B, the former remains dispersionless (pure TO) while the latter, through its coupling with the macroscopic-induced polarization, develops an upward angular dispersion. The observed shift ($\approx$ 2.5 cm^{-1}) is in quite good agreement with the splitting calculated for $\Theta = 45°$ ($\approx$ 3.3 cm^{-1}).

(3) At $\Theta = 45°$ the upward dispersive TO_1 mode is close to the anticrossing with LO_{13}. Both components of the split levels should contribute to the scattering in $z(y',z)y'$ configuration and thus, if unresolved, lead to a peak broader than that due to the $E(x')$ mode [$z(x',z)y'$ configuration].

(4) The smaller peaks observed in $z(x',x')y'$ and $z(y',z)y'$ [or $z(x',z)x'$, dashed upper curve] configurations ($\approx$ 268.5 cm^{-1} and $\approx$ 286.5 cm^{-1}, respectively) occur at the frequencies of the "interface modes." As discussed in Sec. II B, both interface modes are partially z and y' polarized (or x' polarized for $\vec{q}$ along the z-x' plane) at $\Theta = 45°$, which explains the observation

of scattering at the two frequencies for the z- and y'-polarized allowed configurations (or x' polarized for light collected along x'). Note that the amplitudes of the LO-like peaks for the two lower spectra are different for light collected along y' or x', existing some transfer of efficiency towards the "forbidden" (lower) configuration for the former. Such distinction between x' and y' may be due to interface steps[36,37] along either [110] or [1$\bar{1}$0] directions which could break k-conservation perpendicular to them. Unfortunately, which of the two perpendicular directions was the [110] and which was the [1$\bar{1}$0] was not determined for our sample.

We now proceed with the description of 90° scattering where the light is incident along z but collected along y. The spectra are shown in Fig. 4 for the same polarization configurations and in the same sequence as those depicted in Fig. 3 for light scattered along y'. The spectra are different from those in Fig. 3, thus demonstrating that the Raman tensors are *not* invariant under rotations about z;[9] in fact, they basically agree with the selection rules derived for D_{2d} symmetry MQW's (also shown in Fig. 4). We note that anisotropy for GaAs/AlAs MQW's in backscattering experiments along [100] and [110] directions was also reported in Refs. 5–8. The following relevant features are revealed in Fig. 4. (i) The dominant scattering mechanism is the deformation potential, leading to stronger scattering of B_2-like than A_1 modes

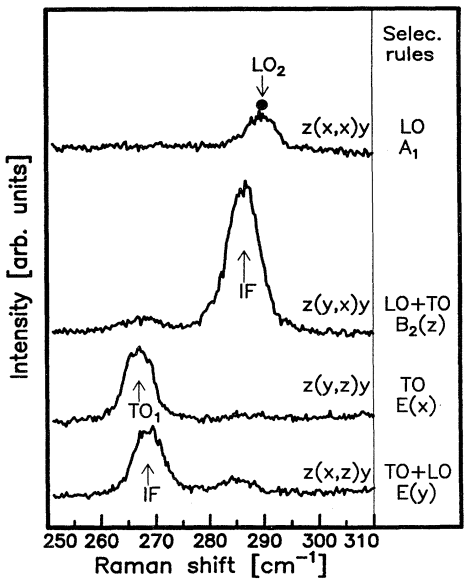

FIG. 4. Raman spectra in right-angle geometry excited at a laser energy of 1.53 eV, with scattered light collected along a [010] direction. The four possible configurations are ordered in the same sequence as those of Fig. 3. The selection rules predicted for D_{2d} symmetry are also indicated, together with the expected character of the modes (see the discussion in Sec. II B). Note that contrary to the spectra in Fig. 3 where the TO-like IF mode is broader than the TO_1 probably to an anticrossing behavior, both peaks appear here roughly with the same width.

(π/d-Fröhlich mediated), as expected.[14,15] (ii) The peak observed for A_1 allowed scattering is at a higher frequency ($\approx$ 290 cm^{-1}) than that observed for B_2 symmetry [$\approx$ 286.5 cm^{-1}, similar to the results obtained in $z(x',x')y'$ configuration in Fig. 3]. In fact, it coincides with the energy calculated for the LO_2 mode in Fig. 1, as expected for A_1 scattering. (iii) The energy position of the TO-like modes in the two lower spectra is inverted with respect to the corresponding ones in Fig. 3: again, the mode polarized perpendicular to the $\vec{q}$-z plane [belonging to $E(x)$ representation for $q = 0$] remains at the bulklike TO frequency while that polarized along y shifts to higher frequency. (iv) Weaker scattering is also observed at the upper (lower) interface mode frequency in the $z(x,z)y$ [$z(y,x)y$] configuration, as expected due to the mixed y and z polarization of that mode for $\Theta = 45°$. Note that no feature in the LO frequency range is observed in this case for the $z(y,z)y$ configuration in accord with the pure TO character of the allowed x-polarized mode.

B. Forward scattering geometry

Before presenting the data, let us discuss how scattering in forward geometry occurs. For forward scattering along [1$\bar{1}$0] the $\vec{q}$ transfer is perpendicular to [1$\bar{1}$0], i.e., it takes place along *any* direction in the x'-z plane. Hence, the excited phonons scan the whole Θ range in Fig. 1 thus contributing a continuum of scattered energies. The Raman spectra must be interpreted consequently in terms of the "angular phonon density of states" weighted by the corresponding scattering efficiency. In this scheme, maxima correspond to frequencies around which a large number of modes exist or, in addition, the scattering efficiency of a particular vibration is large. Also, as pointed out in Ref. 34, the spectra can be strongly affected due to the anticrossings of the interface mode bands with the odd confined modes if the gaps are large enough to be resolved.

The maximum magnitude of q transferred in a forward scattering experiment in *bulk* samples can be calculated from the maximum collecting angle (determined by the collecting lens) and the refractive index of the material. This applies also to our *waveguided structure*: although rays propagating at larger angles in the MQW may be waveguided by the cladding, they are not detected if they leave the sample with an angle larger than that defined by the collecting lens. In our case this angle was about 25° with respect to the lens axis, which gives $\approx$ 7° inside the sample. This leads to a maximum scattered wave vector of approximately $q = 1.7 \times 10^4$. The calculated angular dispersion of GaAs-like optical phonons does not depend too strongly on the magnitude of $\vec{q}$ and for $q = 1.7 \times 10^4$ cm^{-1} and $q = 9.56 \times 10^4$ cm^{-1} the calculated modes are virtually identical. Consequently, we will analyze the forward scattering data also in terms of Fig. 1. Note, however, that for forward scattering along y', phonons are scattered along the x'-z plane and thus $\Theta = 90°$ corresponds to x'.

We show in Fig. 5 forward scattering Raman spec-

tra obtained along [1$\bar{1}$0] for the four possible polarization configurations, together with the corresponding predicted selection rules. The peak positions are indicated in Fig. 1 by open circles. The spectra reveal the following characteristics: (i) the main peaks agree with the selection rules, the z-polarized vibrations corresponding basically to LO-like frequencies and the in-plane modes to TO-like energies; (ii) B_2 modes show larger scattering efficiency than A_1 symmetry ones, thus confirming that the bulklike deformation potential is the dominant scattering mechanism below the E_0 gap;[14,15] (iii) besides the principal peaks, a continuum of scattered frequencies with secondary maxima occurs between the bulklike LO and TO energies with a decreasing amplitude towards the "forbidden" frequency for each configuration.

The main contribution to the scattering efficiency comes, as discussed above, from the nodeless "interface" modes. Correspondingly, the scattering continuum appears shifted to the upper (lower) half of the TO-LO frequency region for the z (x') polarized modes. According to the shape of the interface modes' dispersion the maximum contribution to these continua may be expected at the borders of each of the two bands, corresponding to $\Theta = 0°$ and 90°. In fact, besides the main peaks located approximately at the LO_1 and TO_1 bulklike frequencies, secondary maxima can be distinguished superimposed on the Raman continuum at approximately 280.5 cm^{-1} for $y'(x',x')y'$ and at 276 cm^{-1} for the two $E(x')$ allowed configurations. These two peaks are close to the calculated "interface" modes at $\Theta = 90°$. The fact that the spectra are not symmetric but show instead a marked weight towards the LO_1 and TO_1 bulklike frequencies indicates a predominance of phonons with $\Theta \approx 0°$, suggesting a more efficient collection of light scattered along the z-y' plane. This can be understood as due to the waveguided structure of the sample: light scattered along the z-y' plane is reflected at the MQW-cladding interface and thus brought to the focus of the collecting lens (determined by the output spot on the back part of the sample).

One surprising feature of the data in Fig. 5 is the observation for the $y'(x',x')y'$ configuration of a minor peak at approximately 276.5 cm^{-1}, close to the broader peak observed in $E(x')$ allowed scattering. We can understand this by analyzing the mode displacements of the "interface modes" shown for two values of Θ (45° and 90°) in Fig. 6. The x'-polarized part of the modes is indicated with solid lines, while those polarized along z are represented by dashed lines. As discussed in Sec. II, close to $\Theta = 0°$ LO_1 is predominately z polarized while TO_1 has a strong x' component. Due to the effect of both the macroscopic electric field and the boundary conditions at the GaAs/AlAs interfaces, as Θ increases the $m = 1$ (i.e., interface) vibrations are polarized both along z *and* x'. Moreover, they anticross and mix with higher-order odd confined modes as evidenced by the appearance of a high-frequency component (besides the nodeless one) in the displacements along z (see the curves for $\Theta = 45°$ in Fig. 6). Due to this mixing the upper "interface" mode is "pushed down" by the mixing and the lower one "pushed up." Consequently, the two modes are not

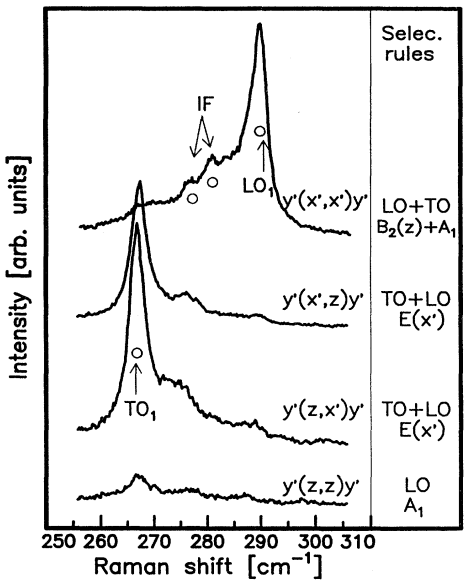

FIG. 5. Raman spectra obtained in forward scattering geometry along [1$\bar{1}$0], with an excitation energy of 1.52 eV. The collection angle *within* the sample is limited to about 7° with respect to the collecting lens axis. The transferred $\vec{q}$ is perpendicular to the light propagation direction. The selection rules predicted for D_{2d} symmetry are also indicated, together with the expected character of the modes (see the discussion in Sec. II B).

degenerate for $\Theta = 90°$, as expected for MQW's with similar well and barrier width from a simple dielectric continuum model,[16] but instead cross close to $\Theta = 90°$. Interestingly, due to this crossing at $\Theta = 90°$ the upper (lower) confined mode turns out to be x' (z) polarized. For our sample the wells are slightly thicker than the bar-

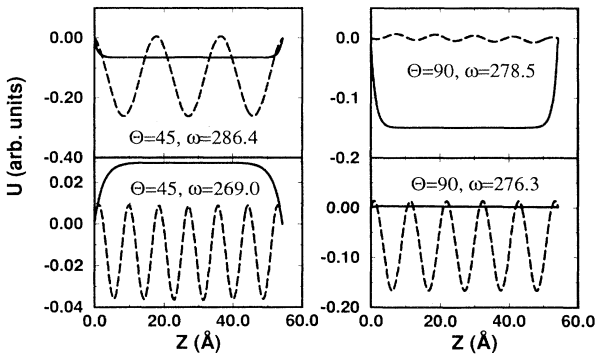

FIG. 6. Atomic displacement of interfacelike modes in a GaAs layer for two values of Θ, 45° and 90° ($\Theta = 90°$ corresponds here to $\vec{q} \parallel x'$). The x' (z) -polarized components of the displacements are indicated with solid (dashed) lines. The respective mode frequencies are also indicated. For $\Theta = 45°$ the higher-energy interfacelike mode is mostly z polarized. The lower-energy one is mainly x' polarized but reveals a large z-polarized nodeless component that mixes with high-order confined modes. For $\Theta = 90°$, the lower (higher) energy mode is mainly z (x') polarized, indicating that a crossing of the interfacelike modes has occurred.

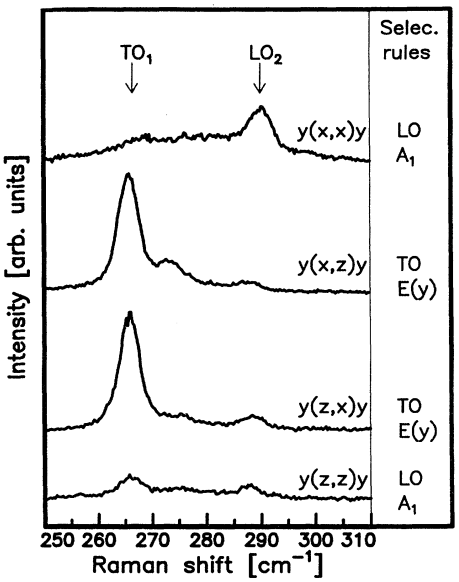

FIG. 7. Raman spectra obtained in forward scattering geometry along [010], with an excitation energy of 1.53 eV. The four possible configurations are ordered in the same sequence as those of Fig. 5. The selection rules predicted for D_{2d} symmetry are also indicated, together with the expected character of the modes (see the discussion in Sec. II B).

riers (51.5 Å and 46 Å, respectively), a fact which contributes to producing the same effect, i.e., a z-polarized mode at a lower energy compared to the x'-polarized one for $\Theta = 90°$. Thus, the peak observed for the $y'(x', x')y'$ configuration at ≈ 276.5 cm^{-1} may arise from scattering of phonons propagating parallel to the layers. Within this picture, the peak at 280.5 cm^{-1} would result instead from scattering close to but not exactly at $\Theta = 90°$.

In Fig. 7 we show forward scattering Raman spectra for light incident along the [010] crystal axis, together with the predicted selection rules. The results agree well with theory: the z-polarized modes correspond to LO-like frequencies while the in-plane polarized vibrations are basically TO-like. Only scattering of z-polarized modes of A_1 symmetry is allowed, which thus appears with reduced intensity. Since the transferred q for forward scattering along y belong to the z-x plane, the $E(y)$ modes should vibrate at the bulklike TO frequencies, i.e., they should correspond to the dispersionless TO_1 mode of Fig. 1. Consequently, no Raman scattering intensity is expected between the bulklike TO and LO frequencies for the two intermediate configurations of Fig. 7. This in fact occurs for $y(z, x)y$ while, on the other hand, an unexpected secondary maximum appears for $y(x, z)y$.

C. Backscattering geometry

We present next our results of Raman scattering in backscattering geometry for light incident on a cleaved (110) face of an unclad GaAs/AlAs MQW. We have measured the Raman spectra for several excitation energies but, for the sake of brevity, we will only present the data taken at 2.41 eV and point out, when important, the features we found to depend on laser frequency. We analyze our data in terms of the angular phonon dispersion of Fig. 1 although it was calculated for a different q ($q \approx 9 \times 10^5$ cm^{-1} for backscattering with 2.41 eV photons). Small differences between the calculated angular dispersions for $q = 9.56 \times 10^4$ cm^{-1} and $q = 9 \times 10^5$ cm^{-1} are only evident at the anticrossings of the $m = 1$ modes with the even numbered ones. Note that, for backscattering along $[1\bar{1}0]$, the transferred $\vec{q}$ is along y' (corresponding to $\Theta = 90°$ in Fig. 1).

In Fig. 8 we show Raman spectra for the four possible configurations, taken with the green line (2.41 eV) of an Ar^+-ion laser (this figure should be compared with Fig. 3 of Ref. 6). The positions of the peaks are indicated in Fig. 1 by full triangles. The spectra reveal the following important features. (i) Peaks at the bulklike TO frequency are observed for the two lower configurations, as expected for x'-polarized modes which do not show dispersion with Θ. (ii) A low-intensity LO-like shoulder close to the LO_2 frequency is observed in the $y'(z, z)y'$ configuration, as expected for allowed A_1 scattering. We note that for this configuration Hessmer *et al.*[6] reported "forbidden" scattering at the TO_1 frequency, something we do not observe. (iii) Strong scattering at the "interface" modes frequency is observed for the $y'(x', x')y'$ configuration, in agreement with the selection rules which predict the excitation of B_2 symmetry phonons. Two peaks are resolved corresponding to the two interface

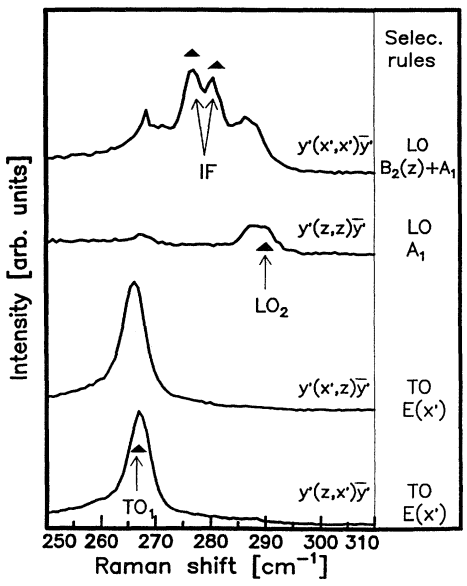

FIG. 8. Raman spectra taken in backscattering geometry with excitation at a laser energy of 2.41 eV (green line of Ar^+ laser). Light was incident along y'. The four possible configurations are shown, together with the predicted selection rules discussed in Sec. II B.

modes at $\Theta = 90°$. The spectral position of these peaks agrees with that of the corresponding configuration in forward scattering along y' [$y'(x',x')y'$ configuration] for which two peaks are also seen. As in that case we argue here that, due to their crossing, close to $\Theta \approx 90°$ both "interface" vibrations have a large z-polarized component. (iv) For the $y'(x',x')y'$ configuration also LO- and TO-like shoulders are observed. They are at a lower and higher frequency, respectively, compared to the bulklike frequencies. This agrees with the calculated angular dispersion which shows that, for $\Theta = 90°$, no signal at the LO_1 frequency is expected. Nevertheless, the LO-like feature is at too low a frequency (≈ 287 cm^{-1}) to be assigned to LO_3. In fact, both features are very close to the position of the interface modes observed for 90° scattering (see Fig. 3). We have not observed any scattering at these frequencies for experiments with excitation at 2.623 eV (blue line of Ar^+-ion laser) nor at 1.916 eV (red line), which suggests that they may be due to resonance effects (probably impurity mediated Fröhlich scattering).[27] We note that scattering at the "forbidden" TO- and LO-like frequencies was also reported for this configuration in Ref. 6, although it was much stronger in that case.

Before concluding we comment on the reasons that may have led to the lack of agreement between theory and experiment in Ref. 9. There may have existed, first of all, quality-related problems in the samples grown several years ago but, beside that, it is possible to speculate on the absence of strict confinement of the GaAs optical modes in the well through interaction with the GaAs-like[38] modes of the barriers. In Ref. 9 barriers with 28% of Al were used and according to existing literature[38] there are LO and TO GaAs-like modes in $Al_xGa_{1-x}As$ at about 286 cm^{-1} and 275 cm^{-1}, respectively (one should take into account that the peaks are also somewhat broader than those of bulk GaAs, making, for example the approximately 4 cm^{-1} difference to the GaAs-phonon of the wells very small). Note that some of the properties studied here depend exclusively on this confinement (like the change from TO to LO character and *vice versa*, mentioned in the Introduction, for in-plane propagation). Apparently, the confinement in the sample of Ref. 9 was enough to unveil the effect of the boundaries on some of the selection rules but not enough to make the interface phonons angular dispersion visible for $\Theta = 45°$. The discrepancy found in Ref. 9 cannot be due to layer thickness. That of Zucker *et al.* is indeed twice as large as ours, a fact which prevents the observation of confined modes in the former but should not affect the selection rules discussed in our work. Actually, the selection rules are often found to be violated (especially near resonance) because of interface roughness. The large $\vec{k}$-interface modes, halfway between LO and TO for equal well-barrier thickness, are then seen. Under equal growth conditions, however, the effects of interface roughness should be weaker in the thicker sample, i.e., that of Zucker *et al.* We have of course no way of comparing the interface perfection of samples grown 10 years ago, at the early stages of MBE technology. On the other hand, because of the large concentration of GaAs in the barriers in Ref. 9 there is a possibility that this may influence the selection rules. This is why we chose to use pure AlAs in the barriers, which was not popular 10 years ago (because of state of the art problems at that time). We mention, however, that the *tetrahedral point group* selection rules are largely preserved in the $Al_xGa_{1-x}As$ alloys and that our conclusions are simply based on these selection rules. Alloying in the barrier should, however, strongly affect the interface modes since it generates GaAs-like modes in the barrier which must be taken into account when applying the boundary conditions. At this point, no realistic calculational methods for this effect are available and one would have to use cumbersome supercell methods involving several statistical alloy atom distributions plus ensemble averages of the results in order to examine this point. This would only affect the interface mode shifts but not the major aspects of the selection rules discussed in the paper. Our results reconcile, from that point of view, experimental findings with theoretical expectations.

V. CONCLUSIONS

We have presented results for Raman scattering spectra of optical phonons in GaAs/AlAs MQW's, for three different *in-plane* scattering geometries: 90°, forward, and backscattering with light propagating along the layers of the heterostructure. We have demonstrated that these Raman spectra are consistent with the selection rules expected from both symmetry grounds and consideration of the way the macroscopic electric fields modify the optical vibrations of a polar MQW structure. Also, we find the phonon energies to be in good agreement with calculations based on a continuum model. The peak intensities confirm that the bulklike deformation potential is the dominant scattering mechanism below the E_0 gap.

ACKNOWLEDGMENTS

Thanks are due to the technical staff of our group (H. Hirt, M. Siemers, and P. Wurster) for expert technical help and to Norbert Esser for his careful reading of a draft version of this paper. A.F. and M.P.C would like to thank the Alexander von Humboldt Foundation and the European Union, respectively, for financial support.

* Present address: Cavendish Laboratory, University of Cambridge, Madingley Road, CB3 OHE, UK.

[1] M. V. Klein, IEEE J. Quantum Electron. **QE-22**, 1760 (1986).

[2] B. Jusserand and M. Cardona, in *Light Scattering in Solids*, edited by M. Cardona and G. Güntherodt (Springer, Berlin, 1989), Vol. 5.

[3] M. Cardona, Superlattices Microstruct. **5**, 27 (1989).

[4] J. Menéndez, J. Lumin. **44**, 285 (1989).
[5] A. Huber, T. Egeler, W. Ettmüller, H. Rothfritz, G. Tränkle, and G. Abstreiter, Superlattices Microstruct. **9**, 309 (1991).
[6] R. Hessmer, A. Huber, T. Egeler, M. Haines, G. Tränkle, G. Weimann, and G. Abstreiter, Phys. Rev. B **46**, 4071 (1992).
[7] G. Scamarcio, M. Haines, G. Abstreiter, E. Molinari, S. Baroni, A. Fischer, and K. Ploog, Phys. Rev. B **47**, 1483 (1993).
[8] M. Zunke, R. Schorer, G. Abstreiter, W. Klein, G. Weimann, and M. P. Chamberlain, Solid State Commun. (to be published).
[9] J. E. Zucker, A. Pinczuk, D. S. Chemla, A. Gossard, and W. Wiegmann, Phys. Rev. Lett. **53**, 1280 (1984).
[10] R. Fuchs and K. L. Kliewer, Phys. Rev. **140**, A2076 (1975).
[11] W. E. Jones and R. Fuchs, Phys. Rev. B **4**, 3581 (1971).
[12] G. Kanellis, J. F. Morhange, and M. Balkanski, Phys. Rev. B **28**, 3406 (1983).
[13] C. Colvard, R. Merlin, M. V. Klein, and A. C. Gossard, Phys. Rev. Lett. **45**, 298 (1980); C. Colvard, T. A. Grant, M. V. Klein, R. Fisher, H. Morkoc, and A. C. Gossard, Phys. Rev. B **31**, 2080 (1985).
[14] B. Jusserand, D. Paquet, and A. Regreny, Phys. Rev. B **30**, 6245 (1984).
[15] A. K. Sood, J. Menéndez, M. Cardona, and K. Ploog, Phys. Rev. Lett. **54**, 2111 (1985).
[16] A. K. Sood, J. Menéndez, M. Cardona, and K. Ploog, Phys. Rev. Lett. **54**, 2115 (1985).
[17] E. Richter and D. Strauch, Solid State Commun. **64**, 867 (1987).
[18] K. Huang and B. Zhu, Phys. Rev. B **38**, 13 377 (1988).
[19] S. Baroni, P. Gianozzi, and E. Molinari, Phys. Rev. B **41**, 3870 (1990).
[20] M. P. Chamberlain, M. Cardona, and B. K. Ridley, Phys. Rev. B **48**, 14 356 (1993).
[21] K. Huang, B. Zhu, and H. Tang, Phys. Rev. B **41**, 5825 (1990).
[22] W. Hayes and R. Loudon, in *Scattering of Light by Crystals* (Wiley, New York, 1978).
[23] J. M. Jacob, D. S. Kim, A. Bouchalkha, J. J. Song, J. F. Klem, H. Hou, C.W. Tu, and H. Morkoç, Solid State Commun. **91**, 721 (1994).
[24] B. Jusserand, F. Alexandre, J. Dubard, and D. Paquet, Phys. Rev. B **33**, 2897 (1986).
[25] M. Cardona, in *Light Scattering in Solids II*, edited by M. Cardona and G. Güntherodt, Topics in Applied Physics Vol. 50 (Springer, Berlin, 1982).
[26] P. Vogl, in *Physics of Nonlinear Transport in Semiconductors*, edited by D. K. Ferry, J. R. Baker, and C. Jacoboni (Plenum, New York, 1980).
[27] J. Menéndez and M. Cardona, Phys. Rev. B **31**, 3696 (1985).
[28] R. M. Martin, Phys. Rev. B **4**, 3676 (1971).
[29] P. K. Tien, Rev. Mod. Phys. **49**, 361 (1977).
[30] H. A. Haus and D. Miller, IEEE J. Quantum Electron. **22**, 310 (1986).
[31] J. S. Weiner, D. S. Chemla, D. A. B. Miller, H. A. Haus, A. C. Gossard, W. Wiegmann, and C. A. Burrus, Appl. Phys. Lett. **47**, 664 (1985).
[32] K. Ogawa, T. Katsuyama, and H. Nakamura, Phys. Rev. Lett. **64**, 796 (1990).
[33] A. Fainstein, P. Etchegoin, P. V. Santos, M. Cardona, K. Tötemeyer, and K. Eberl, Phys. Rev. B **50**, 11 850 (1994).
[34] A. J. Shields, M. Cardona, and K. Eberl, Phys. Rev. Lett. **72**, 412 (1994); M. P. Chamberlain, M. Cardona, and A. J. Shields (unpublished).
[35] M. Cardona, in *Semiconductor Superlattices and Interfaces*, Proceedings of the International School of Physics "Enrico Fermi," Course CXVII, Varenna on Lake Como, 1991 (North-Holland, Amsterdam, 1993).
[36] J. H. Neave, B. A. Joyce, P. J. Dobson, and N. Norton, Appl. Phys. A **31**, 1 (1983).
[37] M. D. Pashley, K. W. Haberen, and J. M. Woodall, J. Vac. Sci. Technol. B **6**, 1468 (1988).
[38] B. Jusserand and J. Sapriel, Phys. Rev. B **24**, 7194 (1981).

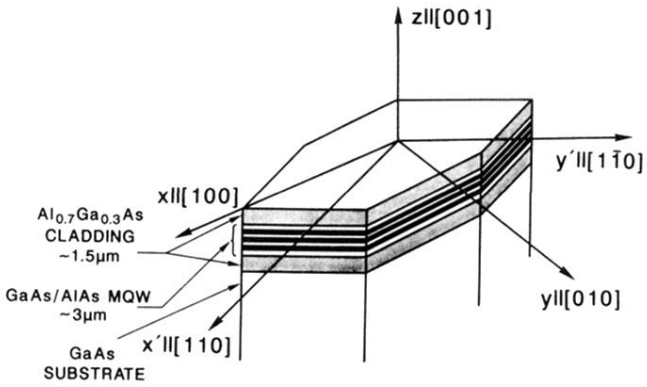

FIG. 2. Schematic of the sample and the coordinate systems used. The sample consists of a thick ($\approx$ 2.8 μm) GaAs/AlAs MQW (300 times 51.5 Å/46 Å) enclosed by $\approx$ 1.5 μm $Al_{0.7}Ga_{0.3}As$ layers. The refractive index of the cladding is smaller than that of the MQW so that light guiding occurs. The axes [110] (x') and [1$\bar{1}$0] (y') are perpendicular to cleavage planes. Some samples were polished perpendicular to the crystalline axes [100] (x) or [010] (y).